Desalination and Water Treatment
www.deswater.com

doi: 10.5004/dwt.2020.26447

207 (2020) 410–419
December

Performance and mechanism of interaction of crystal violet with organohalloysite

Nouria Mahrez[a], Fatiha Bessaha[a,*], Kheira Marouf-Khelifa[a], Ali Çoruh[b], Amine Khelifa[a]

[a]*Laboratoire de Structure, Elaboration et Applications des Matériaux Moléculaires (S.E.A.2M.), Département de Chimie, Université de Mostaganem, B.P. 981, R.P., Mostaganem 27000, Algeria, Tel. +213 61 54 33 94; Fax: +213 45 21 10 18; email: fatiha_bessaha@yahoo.fr (F. Bessaha)*
[b]*Department of Physics, Sakarya University, 54147-Kampus, Sakarya, Turkey*

Received 24 March 2020; Accepted 5 August 2020

ABSTRACT

A series of new organic–inorganic nanohybrid materials were prepared by intercalating dimethylsulfoxide (DMSO) into the interlamellar space of halloysite at different contact times and DMSO/clay ratios. The X-ray diffraction and thermogravimetry/differential thermal analysis studies confirmed the insertion of DMSO into the interlayer space. The increase of the basal spacing to 1.12 nm was thus highlighted for an intercalation rate of 95%. All materials were used to remove crystal violet (CV) from aqueous media. We focused particularly on the mechanism of CV interaction with halloysitic nanohybrids by means of an infrared spectroscopy study. Understanding such an interaction is a fundamental approach for the effective use of halloysitic nanohybrids in wastewater sanitation. pH influence, kinetic, isotherm, and thermodynamic data have been examined. The equilibrium and kinetic data were appropriately adjusted, respectively, by the Redlich–Peterson, and pseudo-second-order models. The amount adsorbed by each nanohybrid depends on the intercalation rate. The larger the intercalated fraction, the better the amount adsorbed, so DMSO is involved in the CV adsorption. The mechanism would involve mainly a hydrogen bond between the electron lone pairs of oxygen of the sulfoxide function and the hydrogen of methyl bound to the tertiary amine of the dye molecule.

Keywords: Nanohybrid; Halloysite; Crystal violet; Mechanism; Hydrogen bond

1. Introduction

A large number of organic and inorganic components present a significant risk for environment as most are difficult to degrade. Crystal violet (CV) is a dye extensively used for textile production or in paper factories, as a biomarker to inhibit the growth of moulds in poultry feed, dermatological agent to reduce the development of digestive problems and fungi,. Regardless of its extensive use, it was identified as a mutagen dye [1].

Different adsorbents were utilized to eliminate CV such as activated carbon [2], nanocomposite [3], and chitosan [4]. In many of these studies, the authors were focused on the performance of CV adsorption through the amount adsorbed and not on the mechanism that controls the CV-material interaction. The mechanistic approach is however a key parameter in understanding environmental pollution.

Nanohybrid materials combining organic and inorganic entities at the molecular scale offer the potential to create a wide variety of new functional surfaces. The layered structure of phyllosilicates addresses this concern by inserting organic compounds into a two-dimensional environment. Halloysite is a quite abundant clay mineral belonging to 1:1 phyllosilicate. The intercalation of organic species into their

* Corresponding author.

interlayer spaces, such as potassium acetate [5], formamide [6], urea [7], hydrazine [8], and hexadecyltrimethylammonium bromide [9], enables to obtain nanohybrids capable of reacting strongly with organic pollutants.

Algerian halloysite intercalated with dimethylsulfoxide (DMSO) at different contact times and DMSO/clay ratios. Several types of halloysite morphologies have been identified such as laminated, fibrous, spheroidal, and tubular [10], so Algerian halloysite would differently interact with DMSO. The resulting materials were characterized by X-ray diffraction (XRD), thermogravimetry/differential thermal analysis (TG/DTA), and transmission electron microscopy (TEM). Thereafter, the raw and intercalated samples were used for the elimination of CV. Different parameters were studied such as pH, contact time, adsorption isotherm, thermodynamic parameters, and infrared (IR) spectroscopy. The aim is to elucidate the mechanism of the CV-halloysitic nanohybrid interaction. The knowledge of such an interaction represents a key approach for the effective application of these materials in wastewater remediation.

2. Materials and methods

2.1. Materials

The material studied is halloysite of Djebel Debbagh. The characterization of the raw material has been previously reported [5,11]. 5.4 g of halloysite were mixed with different volumes of DMSO and contact times (Table 1). The mixture was stirred at 25°C, filtered, and dried at 70°C. The samples were abbreviated to H-DMSO(x): x being the intercalated halloysite fraction (%).

2.2. Characterization

A Philips PW 1830 diffractometer was used for powder XRD (CuKα radiation, 35 mA, 40 kV). Thermal analysis (DTA-TG) was carried out on DT instrument Q 600 TA. An amount of H-DMSO(x) was heated at 10°C min^{-1} with an air flow rate of 50 mL min^{-1}. The infrared spectra were gathered using a Shimadzu Prestige 21 spectrophotometer (Germany) via KBr pellets containing 0.5% of the analyte. TEM images were determined with a JEOL 2100 electron microscope. The clay sample was previously ultrasonically dispersed in ethanol for 5 min.

2.3. Adsorption procedure

A 200 mg L^{-1} CV solution (λ_{max} = 590 nm, Biochem) was prepared. The adsorption experiments were performed by mixing 0.020 g of the material with 0.020 L of the dye solution at different concentrations. The suspension was thereafter centrifuged and analyzed by a Shimadzu 1,240 UV/vis spectrophotometer. Three temperatures were considered: 25°C, 40°C, and 55°C. The operating conditions are summarized in Table 2.

2.4. Theory approach

Pseudo-first-order model [12]:

$$\log\left(Q_e - Q_t\right) = \log Q_e - \frac{K_1 t}{2.303} \tag{1}$$

Pseudo-second-order model [13]:

$$\frac{t}{Q_t} = \frac{1}{K_2 Q_e^2} + \frac{t}{Q_e} \tag{2}$$

$$h = K_2 \cdot Q_e^2 \tag{3}$$

Intraparticle diffusion model [14]:

$$Q_t = K_{id} t^{1/2} + C \tag{4}$$

Table 1
Experimental conditions of crystal violet adsorption

Concentration	20, 40, 60, 100, 150, and 200 mg L^{-1} (solution)/(solid): 1 L g^{-1}, time of contact: 2 h, and pH: 6
pH	2, 4, 6, and 8; C = 40 mg L^{-1}
Kinetics	1, 3, 5, 10, 20, 40, 60, 120, and 240 min; C = 40 mg L^{-1}
Temperature	25°C, 40°C, 55°C (solution)/(solid): 1 L g^{-1}; time of contact: 2 h; pH: 6

Table 2
Intercalation rate according to operating conditions

Sample	Halloysite weight (g)	Intercalating agent	Volume of the solution (mL)	Contact time (h)	Intercalation rate (%)
H	–	–	–	–	0
H-DMSO (95)	5.4	DMSO	54	80	95
H-DMSO (72)	5.4	DMSO-H_2O	86.4–3.6	80	72
H-DMSO (81)	5.4	DMSO	90	40	81
H-DMSO (66)	5.4	DMSO	180	40	66

where Q_t is the quantity fixed in time t (mg g^{-1}), Q_e is the quantity fixed at equilibrium (mg g^{-1}), K_1 is the rate constant (pseudo-first-order) (min^{-1}), K_2 is the rate constant (pseudo-second-order) (g mg^{-1} min^{-1}), C is the intercept, and K_{id} is the rate constant (intraparticle diffusion) (mg g^{-1} min$^{-1/2}$).

Langmuir isotherm [15]:

$$\frac{C_e}{Q_e} = \frac{1}{Q_m \cdot K_L} + \frac{C_e}{Q_m} \tag{5}$$

Freundlich isotherm [16]:

$$\log Q_e = \log K_F + \frac{1}{n}\log C_e \tag{6}$$

Redlich–Peterson isotherm [17]:

$$Q_e = \frac{K_{RP} C_e}{1 + a_{RP} C_e^{\beta}} \tag{7}$$

where C_e is the concentration at equilibrium (mg L^{-1}), K_L is the affinity parameter (L mg^{-1}), Q_m is the quantity fixed in monolayer (mg g^{-1}), K_F is the factor related to the capacity of adsorption (L g^{-1}), $1/n$ is the factor due to the intensity of adsorption, K_{RP} and a_{RP} are the Redlich–Peterson constants, and β is the factor correlated to surface heterogeneity.

$$\ln K_d = \left(\frac{-\Delta H^\circ}{R.T}\right) + \left(\frac{\Delta S^\circ}{R}\right) \tag{8}$$

where ΔH° is the enthalpy change (kJ mol^{-1}), ΔS° is the entropy change (J mol^{-1} K^{-1}).

$$K_d = \frac{Q_e}{C_e} \tag{9}$$

where K_d is the distribution coefficient (L g^{-1}).

$$\Delta G^\circ = \Delta H^\circ - T\Delta S^\circ \tag{10}$$

where ΔG° is the Gibbs energy change (kJ mol^{-1}).

3. Results and discussion

3.1. Characterization

3.1.1. Analysis by XRD

The diffractograms of our materials are gathered in Fig. 1. Raw halloysite shows I_{001} reflection at 7.7 Å and another of low intensity at 10 Å (I_{hh}), representing partly hydrated halloysite. H-DMSO(x) solids show a shift of the basal reflection to the low values of 2θ, synonymous with the insertion of DMSO into the interlayer space with an increase in basal spacing from 7.7 to 11.2 Å. The high intensity of the first-order basal reflection of the inserted phase, I_{i001}, occurs at the detriment of that at 7.7 Å (I_{r001}). The intensity of I_{i001} is not the same for all intercalated samples, which indicates that the proportion of DMSO inserted into halloysite differs according to the operating conditions, so, we calculated the intercalation rate, IR, using the following equation [18]:

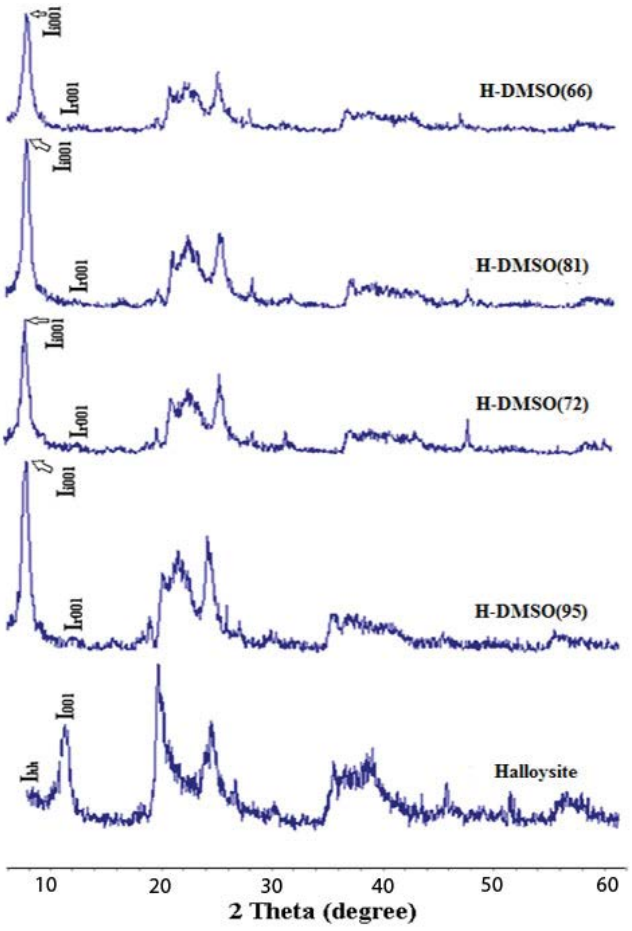

Fig. 1. Diffractograms of halloysite intercalation with DMSO. *I*: intensity; hh: hydrated halloysite; I_{i00l}: basal reflections of interspersed halloysite; I_{r001}: reflection (001) of the remaining unmodified halloysite fraction after intercalation.

$$\mathrm{IR} = \frac{I_{i001}}{\left(I_{i001} + I_{r001}\right)} \tag{11}$$

where I_{i001} is the first-order basal reflection of the intercalated moiety and I_{r001} is the first-order basal reflection of the residual moiety (unmodified phase).

From Table 1, Algerian halloysite was intercalated with DMSO and 72 h were sufficient to attain a rate of 95%. A rate of 62.4% was obtained in the case of kaolinite intercalated by DMSO [19].

3.1.2. TG/DTA analysis

The TG/DTA pattern of the H-DMSO (95) material are shown in Fig. 2. The DTA curve reveals three endothermic peaks at 55°C, 196°C, and 492°C, and an exotherm at 278°C,

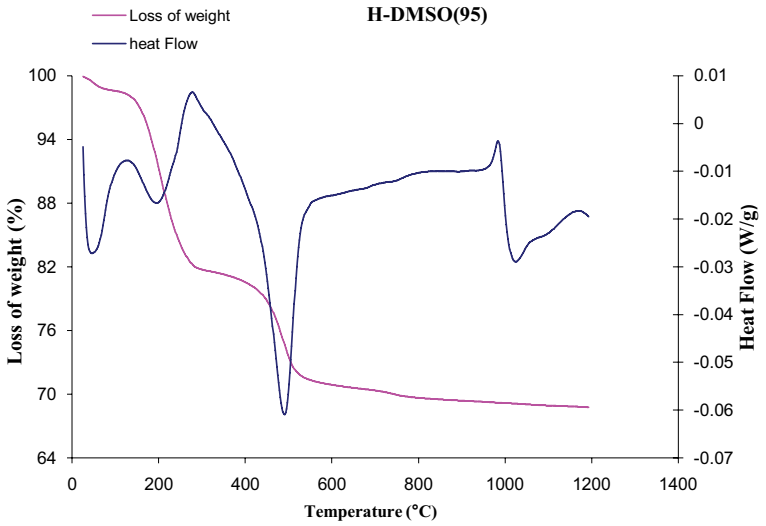

Fig. 2. DTA and TG curves for H-DMSO (95).

in the range 25°C–560°C. The three endothermic peaks are the result of the removal of physically adsorbed water, the release of DMSO from the interlamellar space, and the dehydroxylation of the residual and intercalated phases, respectively. The exothermic peak at 278°C embodies the combustion of the deintercalated DMSO [20], the analysis being conducted under an air flow. These thermal effects are accompanied by a mass loss of 28.5%, corresponding to the loss of physically and chemically bound water, but mostly DMSO.

3.1.3. Transmission electron microscopy

TEM images of the parent halloysite and H-DMSO (95) are shown in Fig. 3. The parent halloysite, H, reveals cylindrical-shaped particles and has a transparent central zone that extends longitudinally along the cylinder, suggesting that the nanotubes are hollow and open. The nanotubes have lengths and diameters quite different. Their outer diameter ranges from 50 to more than 100 nm, while their inner diameter is around 10 nm. This inner diameter coats an open cylindrical cavity called lumen. These rolled tubes consist of several layers of aluminosilicate, bent, and closely packed. In each halloysite nanotube, HNT, the outer surface is composed of siloxane groups (Si–O–Si), while the inner surface is composed of aluminol groups (Al–OH). After intercalation, the H-DMSO (95) image shows nanotubes of different length and diameter. The nanotubes have outer and lumen diameters of 30–100 and 10–20 nm, respectively. Larger diameter tubes have also been identified. The enlargement of the lumen diameter up to 20 nm has a favorable effect on the properties of halloysites in adsorption, immobilization of enzymes, encapsulation of drugs [21].

3.2. Adsorption of crystal violet

3.2.1. pH effect

The effect of pH is displayed in Fig. 4, the concentration being 40 mg L^{-1}. The uptake increases until pH 6 beyond which it remains practically constant. The same evolution was achieved by Masoumi et al. [22] in the adsorption of CV onto a biomaterial. For H-DMSO (95), it increases from 7.1 to 39.5 mg g^{-1}, between 2 and 6.

CV is a basic dye and has a pKa value of 0.8. Due to this low pKa value, it is ionized in the pH range studied and exists as a cationic species. The ionic state and color of CV in aqueous solutions varies with pH. Up to 2, the CV form changes from CV^{3+} (yellow color) to CV^{2+} (blue color). Between 2 and 9, it changes from CV^{2+} to CV^{+} (violet color), the latter color occurring at pH around 7. The aqueous solution of CV turns colorless and is in the form of CV-OH at pH > 9 [23]. In a previous paper [5], we showed that the zeta potential of crude halloysite decreases from –43.54 to –56.44 mV when the pH increases from 6 to 8. A more negative surface is expected to adsorb a greater amount of CV^{+}, the only form existing in the 6–8 range (+1). Since the amount adsorbed is fairly constant in this range (Fig. 4), the electrostatic interaction is unlikely to be the main component governing the CV^{+}-halloysitic clay interaction, at least for organohalloysite samples. Based on the structure of the adsorbate and the surface properties of the adsorbent, the mechanism of removal of CV^{+} by the organoclay could involve hydrogen bonding [24]. Due to its lack of labile hydrogen atoms, DMSO acts only as a proton acceptor [25]. As a result, hydrogen bonds would be formed between the oxygen atoms of DMSO and a proton donator moeity of CV^{+}, which will be discussed in the mechanism section.

3.2.2. Kinetics

The influence of contact time on adsorption is shown in Fig. 5. Kinetics is fast in the first 10 min, decreases then, and tends toward zero after 2 h of contact. The equilibrium of adsorption is thus reached after 2 h of stirring. A similar evolution was obtained by Belkassa et al. [26] in the case of the removal of crystal violet by modified halloysite.

The rate of CV uptake can be described using various kinetic models. The results are listed in Table 3. The pseudo-first-order equation is inappropriate because the

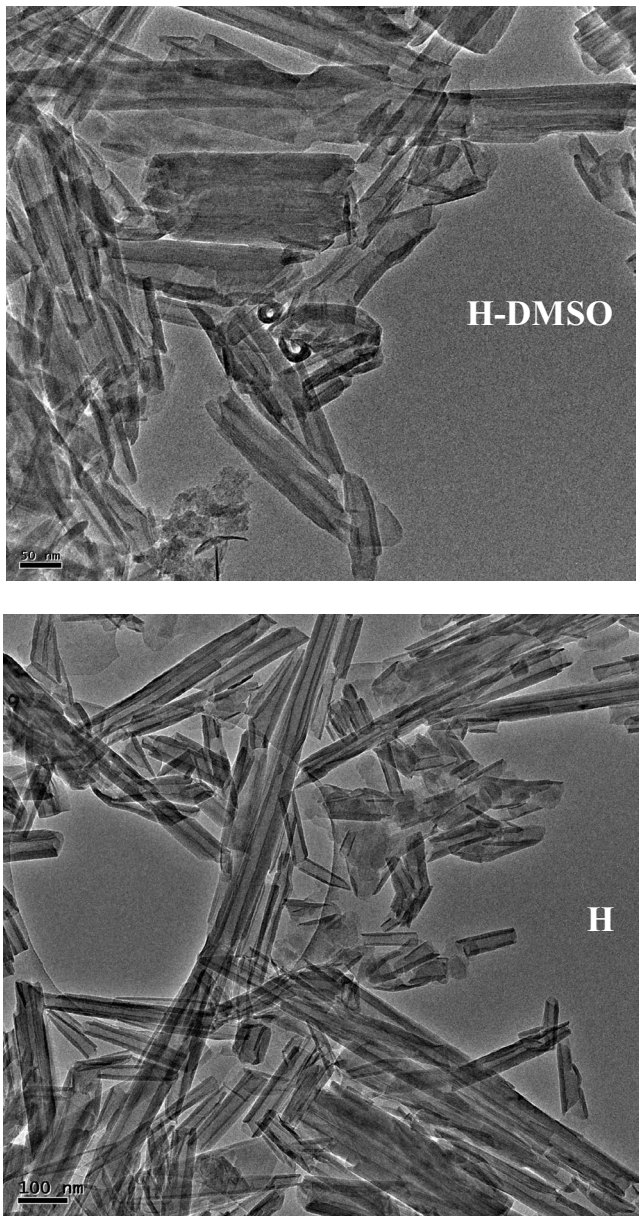

Fig. 3. Transmission electron microscopy images of the crude halloysite, H, and H-DMSO (95).

determination coefficient values are less than 0.90. The pseudo-second-order equation is the most appropriate based on high R^2 values. Also, the experimental ($Q_{e,\exp}$) and calculated ($Q_{e,\text{cal}}$) adsorption capacities are closely related, confirming once again its validity [27]. When batch adsorption is used, the assumption that intraparticle diffusion governs the adsorption mechanism is conceivable. If this happens, the curve Q_t against $\sqrt{t}$ must be a straight line, and if it passes by origin, intraparticle diffusion is the sole process that controls the adsorption mechanism. Knowing that R^2 is ³0.94, this model is also applicable. Since the values of C are different from 0, namely 18.2 and 29.8 mg g^{-1} for H and H-DMSO (95), respectively, intraparticle diffusion is not the unique limiting stage, another process such as external diffusion may also be involved.

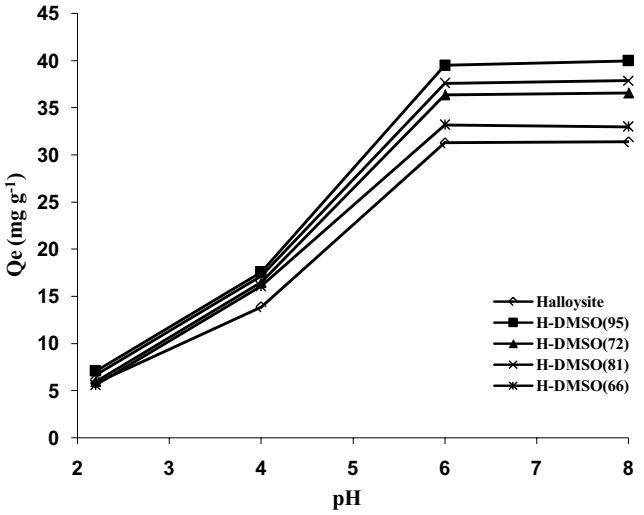

Fig. 4. Effect of pH on CV adsorption by unmodified and DMSO-intercalated halloysites.

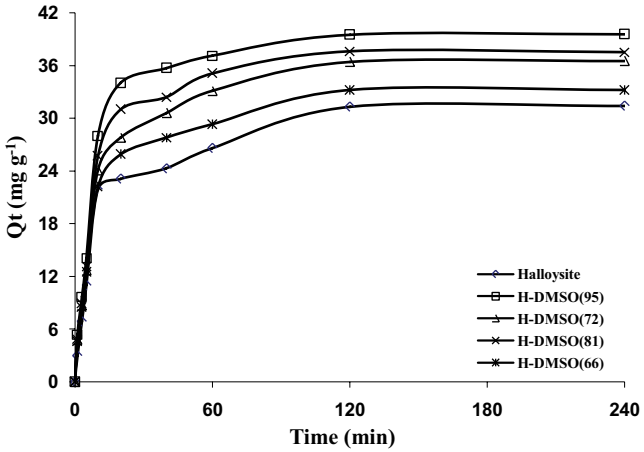

Fig. 5. Adsorption kinetics of CV on unmodified and DMSO-intercalated halloysites.

3.2.3. Isotherms at equilibrium

The isotherms of the adsorption of crystal violet established at different temperatures are illustrated in Fig. 6. For the purpose of this study, we have presented only those of H-DMSO (95). The amount adsorbed declines with increasing temperature, independently of the material examined. As an illustration, H-DMSO (95) adsorbs, at 25°C and 55°C, 94 and 70 mg g^{-1}, respectively. So, an increase in temperature significantly reduces the efficiency of H-DMSO(x). The interaction mechanism of the CV/H-DMSO(x) systems would be of physical nature.

3.2.4. Affinity

The affinity of our materials vis-à-vis crystal violet at 25°C is presented in Fig. 7. The evolution is as follows: H-DMSO (95) > H-DMSO (81) > H-DMSO (72) > H-DMSO (66) > crude halloysite, that is, in accordance with the intercalated fraction. A similar sequence was observed at 40°C

Table 3
Kinetic parameters for CV adsorption onto modified halloysites

Samples		Pseudo-first-order model			Pseudo-second order model				Intraparticle diffusion model		
	$Q_{e,exp}$ (mg g^{-1})	$Q_{e,cal}$ (mg g^{-1})	K_1 (min^{-1})	R^2	$Q_{e,cal}$ (mg g^{-1})	K_2 (g mg^{-1} min^{-1})	h (mg g^{-1} min^{-1})	R^2	K_{id} (mg g^{-1} min$^{-1/2}$)	C (mg g^{-1})	R^2
H	31.3	22.66	0.0297	0.7949	32.46	0.0037	3.91	0.9970	1.048	18.19	0.9362
H-DMSO (95)	39.5	28.3	0.0472	0.8773	40.65	0.0044	7.37	0.9986	0.946	29.76	0.9996
H-DMSO (72)	36.4	27.49	0.0386	0.9093	38.61	0.0042	6.34	0.9985	1.614	20.53	0.9981
H-DMSO (81)	37.6	28.03	0.0437	0.8996	37.59	0.0039	5.52	0.9984	1.228	25.24	0.9354
H-DMSO (66)	33.2	23.83	0.0347	0.8553	34.13	0.0045	5.24	0.9984	1.038	21.25	0.9999

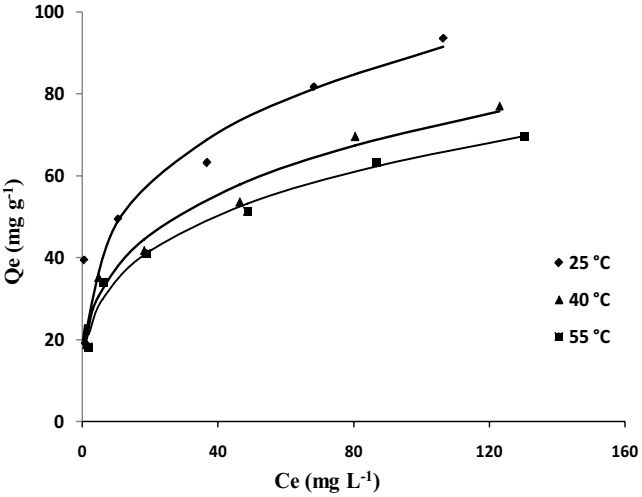

Fig. 6. Adsorption isotherms of crystal violet, according to the experimental data (…) and RP model (—), by H-DMSO (95).

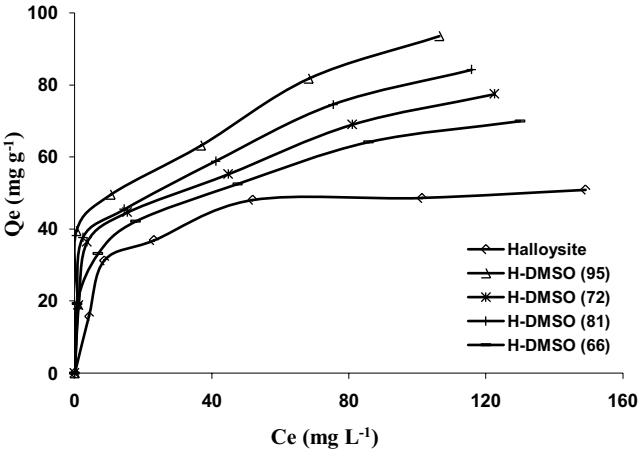

Fig. 7. Adsorption affinity of CV on unmodified and DMSO-intercalated halloysites.

and 55°C. Unmodified halloysite adsorbed 50.9 mg g^{-1} of CV^+ at 25°C. As discussed from TEM analysis, the external surface is composed of siloxane groups (Si–O–Si), while the internal lumen surface is composed of aluminol groups (Al–OH). As the isotherms at equilibrium was performed at pH 6, the external surface is negatively charged, while the inner one is positively charge [25]. Thereby, the adsorption of CV^+ on the crude halloysite is primarily influenced by the electrostatic attraction between positively charged molecules and negatively charged external surface sites. The adsorption of malachite green, a cationic dye, on raw halloysite has also been explained via similar interactions [28]. At 25°C, H-DMSO (95) adsorbs almost twice that the non-intercalated halloysite. In other words, in addition to electrostatic attraction, the intercalating agent, DMSO, would be involved in some way in the dye binding. It adsorbs 94 vs. 50.9 mg g^{-1} for crude halloysite. Other publications highlighted the influence of transforming halloysite into organohalloysite, on adsorption capacity [29,30].

3.2.5. Adsorption capacity of different materials

Table 4 highlights the quantities of crystal violet adsorbed at saturation for different adsorbents. H-DMSO (95) is proving to be a better adsorbent than materials like nanocomposite, kaolin, hydrogel, and charcoal.

3.2.6. Fitting the experimental data with various models

Table 5 presents the fitting parameters of the Langmuir, Freundlich, and Redlich–Peterson models. A model is validated from the parameters determination coefficient (R^2), average relative error (E%), and the adequacy between experimental and theoretical maximum adsorbed quantities. The Langmuir equation does not describe the experimental isotherms of the intercalated samples, because the E(%) values are >10%.

The Freundlich model does not apply to non-intercalated halloysite, due to the values of R^2 and E(%), unlike H-DMSO(x). For the latter, they are >0.94% and <10%, respectively. The parameter K_F reflects the adsorption capacity. It decreases as temperature rises, whatever the sample, in accordance with the experiment results. The exponential coefficient, n, remains fairly constant with temperature. As it characterizes the intensity of adsorption, its relative change proves that the interaction of CV with H-DMSO(x) uses the same components, probably the functional groups that compose DMSO.

The Redlich–Peterson equation includes three factors and uses non-linear regression. It is applicable to homogeneous and heterogeneous adsorption. As seen from Table 5, this equation provides a satisfactory description of the crystal violet adsorption onto H and H-DMSO(x). The experimental and theoretical isotherms derived from the Redlich–Peterson equation are given in Fig. 6. At 25°C, the K_{RP} values decrease according to the sequence: H-DMSO (95) > H-DMSO (81) > H-DMSO (72) > H-DMSO (66) > unmodified halloysite, that is, in full agreement with the affinity series. Note that the values of K_{RP} decline as temperature increases for H-DMSO(x). The values of the β parameter range from 0 to 1 for H-DMSO(x), indicating favorable adsorption.

3.2.7. Thermodynamic parameters

The thermodynamic factors are presented in Table 6. Negative values of $\Delta G°$ highlight the spontaneous character of adsorption. Whatever temperature, spontaneity varies as follows: H-DMSO (95) > H-DMSO (81) > H-DMSO (72) > H-DMSO (66) > unmodified halloysite. Negative values of $\Delta H°$ show that the elimination of CV is exothermic. Adsorption is then unfavored by a temperature elevation. In addition, the adsorbate-adsorbent system is much more orderly ($\Delta S° < 0$). The combination of the parameters $\Delta G° < 0$,

Table 4
Comparison of uptake capacities of CV^+ for various adsorbents

Adsorbents	Q_m (mg g^{-1})	Reference
Nanocomposite	1.9	[31]
Polyacrylamide–kaolin	23.8	[32]
Hydrogels	35.1	[33]
Kaolin	47.3	[34]
Charcoal	58.1	[35]
Magnetic nanocomposite	81.7	[36]
H-DMSO (95)	94	This study

Table 5
Adjustable parameters of the Langmuir, Freundlich, and Redlich–Peterson models

Samples			Langmuir model				Freundlich model				Redlich-Peterson model				
	T (°C)	Q_e (mg g^{-1})	Q_m (mg g^{-1})	K_L (L mg^{-1})	R^2	E (%)	K_F (L g^{-1})	n	R^2	E (%)	K_{rp} (L g^{-1})	β	a_{RP} (mg L^{-1})$^{-0}$	R^2	E (%)
	25	50.90	53.5	0.12	0.999	6.1	13.4	3.4	0.844	15.1	6.53	1.01	0.12	0.974	7.0
H	40	41.65	43.3	0.14	0.999	5.2	12.6	3.8	0.813	14.4	4.84	1.07	0.08	0.992	4.1
	55	35.63	38.2	0.05	0.991	8.0	7.7	3.3	0.941	6.2	5.15	0.83	0.34	0.971	5.4
	25	93.55	94.3	0.14	0.974	23.4	24.2	3.5	0.947	14.1	475.41	0.73	17.95	0.971	9.1
H-DMSO (95)	40	77.06	80.6	0.09	0.975	23.2	19.7	3.6	0.974	5.8	382.24	0.72	19.00	0.984	5.7
	55	69.53	73.0	0.09	0.986	17.1	17.0	3.4	0.967	5.9	355.50	0.73	19.08	0.983	5.9
	25	77.42	79.4	0.11	0.982	22.1	21.0	3.7	0.951	7.1	124.21	0.77	5.04	0.980	7.2
H-DMSO (72)	40	64.09	67.1	0.01	0.987	19.9	19.4	4.2	0.992	3.4	115.90	0.77	5.71	0.991	5.4
	55	55.05	57.8	0.11	0.996	13.8	16.7	4.0	0.986	4.2	43.24	0.81	2.00	0.990	3.1
	25	84.16	86.2	0.12	0.977	27.9	24.1	3.9	0.948	8.0	465.73	0.76	18.17	0.974	9.2
H-DMSO (81)	40	71.61	73.0	0.09	0.978	22.1	19.2	3.8	0.990	4.1	369.40	0.74	18.81	0.993	4.4
	55	60.07	62.1	0.12	0.995	15.3	18.1	4.0	0.985	4.4	51.60	0.81	2.20	0.990	2.2
	25	69.96	72.5	0.11	0.987	19.2	20.8	4.1	0.998	1.9	115.10	0.77	5.14	0.993	4.1
H-DMSO (66)	40	57.35	59.2	0.11	0.992	17.4	18.8	4.4	0.991	1.7	107.50	0.79	5.27	0.984	3.9
	55	47.46	49.5	0.12	0.995	15.1	17.0	4.2	0.983	4.1	95.70	081	5.03	0.981	3.0

Table 6
Thermodynamic parameters for the CV adsorption onto raw and intercalated halloysites

Samples	$\Delta H°$ (kJ mol^{-1})	$\Delta S°$ (kJ mol K^{-1})	$\Delta G°$ (kJ mol^{-1})		
			25°C	40°C	55°C
H	–29.69	–0.088	–3.35	–2.02	–0.69
H-DMSO (95)	–28.38	–0.073	–6.69	–5.60	–4.51
H-DMSO (72)	–29.43	–0.080	–5.47	–4.27	–3.06
H-DMSO (81)	–35.00	–0.096	–6.54	–5.11	–3.68
H-DMSO (66)	–13.65	–0.033	–3.85	–3.35	–2.86

$\Delta H° < 0$, and $\Delta S° < 0$ shows that the removal of crystal violet by H-DMSO(x) is spontaneous at low temperatures.

3.3. FTIR analysis

The infrared spectra are depicted in Fig. 8. The unmodified clay (Fig. 8, Halloysite) shows the 3,704 and 3,632 cm^{-1} bands, due to the vibration of the internal-surface- and internal hydroxyl groups [37]. The 3,436 and 1,626 cm^{-1} bands are caused by the interlayer water stretch and hydration of dAlOH, respectively. The 1,042 and 1,081 cm^{-1} bands are assigned to Si–O–Si and apical Si–O stretches, respectively. The peak at 760 cm^{-1} is ascribed to Si–O–Al stretching, while those at 922, 682, 484, and 548 cm^{-1} are caused by Al–OH, Al–OH, Si–O–Si, and Al–O bends, respectively [38].

When DMSO is inserted into the interlayer space of halloysite, important modifications take place. The intercalation reaction breaks the original hydrogen bond and reveals a new one, which modifies the intensity and frequency of vibration (Fig. 8, H-DMSO (95)). Based on the redshift of the bands to 3,701 and 3,626 cm^{-1} and their decrease in intensity, new hydrogen bondings are created between the sulfoxide groups of DMSO and inner surface OHs. The broadband at 3,448 cm^{-1} is caused by the OH-stretching mode of adsorbed water. The insertion of DMSO into the interlayer is supported by the redshift of the band of Al–OH interlamellar groups to 910 cm^{-1} [39]. Ditto, the redshift of the bands to 752, 677, and 540 cm^{-1} indicates the involvement of the internal surface Al–OHs in the intercalation of DMSO. The reduction in the 1,085 cm^{-1} peak intensity suggests that the intercalated DMSO molecules bind to tetrahedral silicon through their methyl groups [40].

The crystal violet molecule spectrum is shown in Fig. 8, CV. The 1,587 cm^{-1} band is due to the C=C stretch of the benzene ring. The presence of different bands in the range 1,500–500 cm^{-1} reveals mono and para-disubstituted benzene nuclei in the CV dye [41]. The 1,176 cm^{-1} band is ascribed to N–CH_3 stretch [42], while the vibration of aromatic tertiary amine C-N is observed at 1,361 cm^{-1} [36].

After adsorption of crystal violet, significant changes are observed (Fig. 8, CV-loaded H-DMSO (95)). Some peaks shift while others vanish. The bands at 3,701 and 3,626 cm^{-1} reduce in intensity and redshift after adsorption of CV. The intensity of 3,452 cm^{-1} band becomes strong and broad after adsorption, indicating intermolecular H-bonds [6]. The bands at 1,361 and 1,030 cm^{-1} decrease in intensity and shift slightly after adsorption, indicating a strong involvement of the C-N (tertiary amine) and S=O

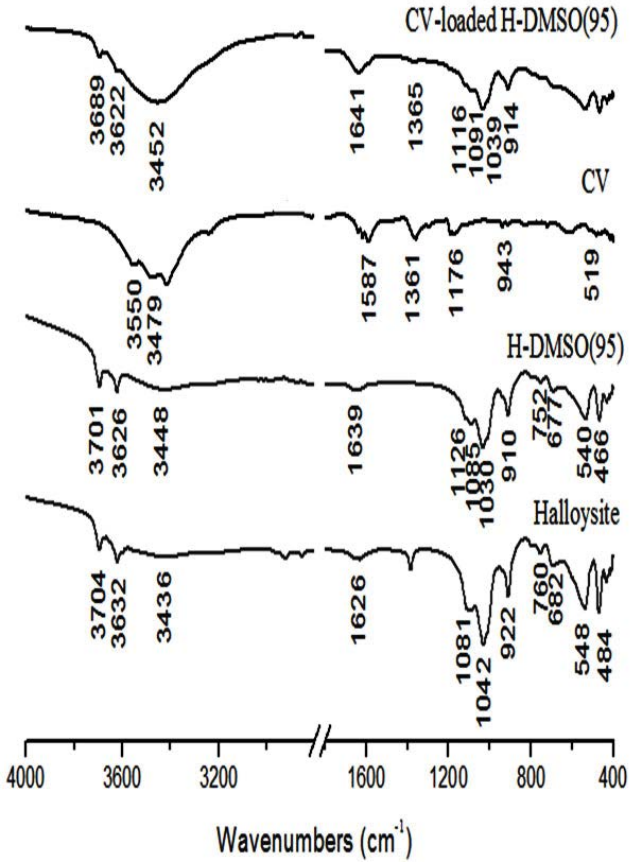

Fig. 8. FTIR spectra of H, H-DMSO (95), CV, and CV-loaded H-DMSO (95).

species. In this line, the disappearance of the 1,176 cm^{-1} band (N-CH_3) after adsorption of CV also confirms the involvement of tertiary amine via the methyl group.

3.4. Adsorption mechanism

Based on the FTIR analysis performed before and after adsorption of this triphenylemethane dye, the interaction mechanism would most likely involve a hydrogen bond. Another feature that supports this type of interaction is the physical nature of adsorption with an exothermic and spontaneous process. Also, hydrogen bond is disrupted and weakens with increasing temperature, which is the case

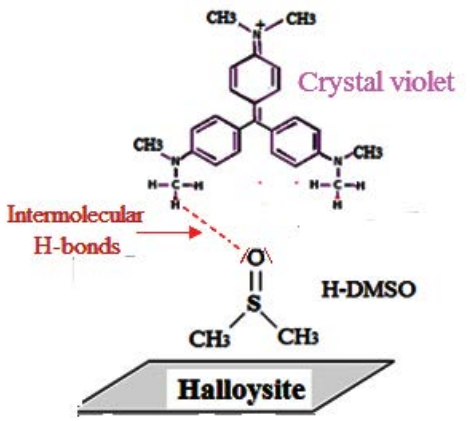

Fig. 9. Mechanism of CV^+ adsorption on H-DMSO (95) via hydrogen bond.

in this study where the adsorbed amount decreases with increasing temperature.

The spectroscopic study also revealed DMSO's involvement in the interaction mechanism via the S=O groups. The adsorption mechanism of CV onto intercalated halloysite with DMSO (95) is given in Fig. 8. DMSO is not a donor but an acceptor of hydrogen [43], a consequence of the strong acceptor character of the hydrogen bonding of DMSO, through the lone pairs of electrons on the oxygen atom [44]. The mechanism of crystal violet adsorption by H-DMSO (95) would involve a hydrogen bonding between the hydrogen of the methyl group bound to the tertiary amine and the oxygen of the sulfoxide group. The same evolution was observed during the adsorption of CV by layered double hydroxides [45]. This interaction is probably not unique but would be associated, to a lesser extent, with electrostatic attraction between positively charged molecules and negatively charged external surface sites, as shown from the pH study. The mechanism of CV^+ adsorption on H-DMSO (95) via hydrogen bond is given in Fig. 9.

4. Conclusion

The intercalation of halloysite with DMSO under different operating conditions was checked by XRD and thermal analysis. The inserted moiety achieved 95% for a basal spacing of 11.2 Å. Adsorption of crystal violet followed the sequence: H-DMSO (95) > H-DMSO (81) > H-DMSO (72) > H-DMSO (66) > unmodified clay, that is, in accordance with the intercalated fraction. H-DMSO (95) adsorbed almost twice that the unmodified halloysite. The process revealed a physical interaction of spontaneous nature at low temperature. The interaction mechanism would involve mainly a hydrogen bond between oxygen from the sulfoxide group and hydrogen from the methyl group belonging to crystal violet.

References

[1] K. Mohanty, J.T. Naidu, B. Meikap, M. Biswas, Removal of crystal violet from wastewater by activated carbons prepared from rice husk, Ind. Eng. Res., 45 (2006) 5165–5171.
[2] F. Nasiri, M. Azad Ghaedi, K. Dashtian, S. Hajati, V. Pezeshkpour, Ultrasonically assisted hydrothermal synthesis of activated carbon-HKUST-1-MOF hybrid for efficient simultaneous ultrasound-assisted removal of ternary organic dyes and antibacterial investigation: taguchi optimization, Ultrason. Sonochem., 31 (2016) 383–393.
[3] A. Kakar, E. Jayamani, M.K.B. Bakri, M.R. Rahman, Chapter 8 - Biomedical and Packaging Application of Silica and Various Clay Dispersed Nanocomposites, M.R. Rahman, Ed., Silica and Clay Dispersed Polymer Nanocomposites Preparation, Properties and Applications, Silica and Clay Dispersed Polymer Nanocomposites, Woodhead Publishing, 2018, pp. 109–136.
[4] A. Kausar, K. Naeem, T. Hussain, Z.H. Nazli, H.N. Bhattic, F. Jubeen, A. Nazi, M. Iqbal, Preparation and characterization of chitosan/clay composite for direct Rose FRN dye removal from aqueous media: comparison of linear and non-linear regression methods, J. Mater. Res. Technol., 8 (2019) 1161–1174.
[5] S. Mellouk, S. Cherifi, M. Sassi, K. Marouf-Khelifa, A. Bengueddach, J. Schott, A. Khelifa, Intercalation of halloysite from Djebel Debagh (Algeria) and adsorption of copper ions, Appl. Clay Sci., 44 (2009) 230–236.
[6] N. Salahuddin, S. Abo-El-Enein, A.A Selim, O. Salah El-Dien, Synthesis and characterization of polyurethane/organo-montmorillonite nanocomposites, Appl. Clay Sci., 47 (2010) 242–248.
[7] F. Tezcan, E. Günister, G. Özen, F.B. Erim, Biocomposite films based on alginate and organically modified clay, Int. J. Biol. Macromol., 50 (2012) 1165–1168.
[8] E.S. Goda, M.A. Gab-Allah, B.S. Singu, K.R. Yoon, Halloysite nanotubes based electrochemical sensors: a review, Microchem. J., 147 (2019) 1083–1096.
[9] K. Mehdi, S. Bendenia, G.L. Lecomte-Nana, I. Batonneau-Gener, F. Rossignol, K. Marouf-Khelifa, A. Khelifa, A new approach about the intercalation of hexadecyltrimethylammonium into halloysite: preparation, characterization, and mechanism, Chem. Pap., 73 (2019) 131–139.
[10] E. Joussein, S. Petit, J. Churchman, B. Theng, D. Righi, B. Delvaux, Halloysite clay minerals – a review, Clay Miner., 40 (2005) 383-426.
[11] F. Bessaha, K. Marouf-Khelifa, I. Batonneau-Gener, A. Khelifa, Characterization and application of heat-treated and acid-leached halloysites in the removal of malachite green: adsorption, desorption, and regeneration studies, Desal. Water Treat., 57 (2016) 14609–14621.
[12] S. Lagergren, About the theory of so-called adsorption of soluble substances, Kungl. Svenska Vetenskapsad, Handl., 24 (1898) 1–39.
[13] Y.S. Ho, G. McKay, Pseudo-second order model for sorption processes, Process Biochem., 34 (1999) 451–465.
[14] W.J. Weber, J.C. Morris, Kinetics of adsorption on carbon from solution, J. Sanitary Eng. Div. Am. Soc. Civ. Eng., 89 (1963) 31-59.
[15] I. Langmuir, Adsorption of gases on plane surfaces of glass, mica and platinum, J. Am. Chem. Soc., 40 (1918) 1361–1403.
[16] H.M.F. Freundlich, Over the adsorption in solution, J. Phys. Chem., 57 (1906) 385–470.
[17] O. Redlich, D.L. Peterson, A useful adsorption isotherm, J. Phys. Chem., 63 (1959) 1024–1033.
[18] A. Wiewióra, G.W. Brindley, Potassium Acetate Intercalation in Kaolinites and Its Removal: Effect Of Material Characteristics, L. Heller, Ed., Proceedings of the International Clay Conference Tokyo, Israel University Press, Jerusalem, 1969, pp. 723–733.
[19] J.A. Mbey, F. Thomas, C.J. Ngally Sabouang, S. Liboum, D. Njopwouo, An insight on the weakening of the interlayer bonds in a Cameroonian kaolinite through DMSO intercalation, Appl. Clay Sci., 83 (2013) 327–335.
[20] H. Cheng, Q. Liu, J. Yang, S. Ma, R.L. Frost, The thermal behavior of kaolinite intercalation complexes – a review, Thermochim. Acta, 545 (2012) 1–13.
[21] M. Tharmavaram, G. Pandey, D. Rawtani, Surface modified halloysite nanotubes: a flexible interface for biological, environmental and catalytic applications, Adv. Colloid Interface Sci., 261 (2018) 82–101.

[22] A. Masoumi, K. Hemmati, M. Ghaemy, Low-cost nanoparticles sorbent from modified rice husk and a copolymer for efficient removal of Pb(II) and crystal violet from water, Chemosphere, 146 (2016) 253–262.
[23] L.M. Cotoruelo, M.D. Marques, F.J. Dıaz, J. Rodrıguez-Mirasol, J.J. Rodrıguez, T. Cordero, Lignin-based activated carbons as adsorbents for crystal violet removal from aqueous solutions, Environ. Prog. Sustainable Energy, 31 (2012) 386–396.
[24] I. Loulidi, F. Boukhlifi, M. Ouchabi, A. Amar, M. Jabri, A. Kali, S. Chraibi, C. Hadey, F. Aziz, Adsorption of crystal violet onto an agricultural waste residue: kinetics, isotherm, thermodynamics, and mechanism of adsorption, Sci. World J., 2020 (2020), doi: 10.1155/2020/5873521.
[25] D. Tan, P. Yuan, D. Liu, P. Du, Surface Modifications of Halloysite, P. Yuan, A. Thill, F. Bergaya, Eds., Nanosized Tubular Clay Minerals - Halloysite and Imogolite, Elsevier, 2016, pp. 167–201.
[26] K. Belkassa, F. Bessaha, K. Marouf-Khelifa, I. Batonneau-Gener, I.D. Comparot, A. Khelifa, Physicochemical and adsorptive properties of a heat-treated and acid-leached Algerian halloysite, Colloids Surf., A, 421 (2013) 26–33.
[27] F. Bessaha, N. Mahrez, S. Bendenia, F. Kasmi, K. Marouf-Khelifa, A. Khelifa, Characterization and spectroscopic study of a heat-treated and acid-leached halloysite used in Congo red adsorption, Int. J. Intell. Eng. Syst., 10 (2017) 272–279.
[28] G. Kiani, M. Dostali, A. Rostami, A.R. Khataee, Adsorption studies on the removal of Malachite Green from aqueous solutions onto halloysite nanotubes, Appl. Clay Sci., 54 (2011) 34–39.
[29] A. Wscislo, J. Matusik, Halloysite-based material with improved cation sorption properties, Geol. Geophys. Environ., 38 (2012) 553-554.
[30] P. Maziarz, J. Matusik, The kinetics of heavy metals immobilization by modified halloysite, Geol. Geophys. Environ., 40 (2014) 108–109.
[31] M.K. Satapathy, P. Das, Optimization of crystal violet dye removal using novel soil-silver nanocomposite as nanoadsorbent using response surface methodology, J. Environ. Chem. Eng., 2 (2014) 708–714.
[32] S.R. Shirsath, A.P. Patil, B.A. Bhanvase, S.H. Sonawane, Ultrasonically prepared poly (acrylamide)-kaolin composite hydrogel for removal of crystal violet from wastewater, J. Environ. Chem. Eng., 3 (2015) 1152–1162.
[33] S. Li, Removal of crystal violet from aqueous solution by sorption into semi-interpenetrated networks hydrogels constituted of poly (acrylic acid-acrylamide-methacrylate) and amylose, Bioresour. Technol., 101 (2010) 2197–2202.
[34] B.K. Nandi, A. Goswami, M.K. Purkait, Removal of cationic dyes from aqueous solutions by kaolin: kinetic and equilibrium studies, Appl. Clay Sci., 42 (2009) 583–590.
[35] S. Kaur, S. Rani, R.K. Mahajan, Adsorptive removal of dye crystal violet onto low-cost carbon produced from eichhornia plant: kinetic, equilibrium, and thermodynamic studies, Desal. Water Treat., 53 (2013) 543–556.
[36] K.P. Singh, S. Gupta, AK. Singh, S. Sinha, Optimizing adsorption of crystal violet dye from water by magnetic nanocomposite using response surface modeling approach, J. Hazard. Mater., 186 (2011) 1462–1473.
[37] F. Bessaha, N. Mahrez, K. Marouf-Khelifa, A. Çoruh, A. Khelifa, Removal of Congo red by thermally and chemically modified halloysite: equilibrium, FTIR spectroscopy, and mechanism studies, Int. J. Environ. Sci. Technol., 16 (2019) 4253–4260.
[38] S. Zhang, Q. Liu, H. Cheng, F. Zeng, Combined experimental and theoretical investigation of interactions between kaolinite inner surface and intercalated dimethyl sulfoxide, Appl. Surf. Sci., 331 (2015) 234–240.
[39] K.S. Abou-El-Sherbini, A.M. Elzahany, Eman, A. Wahba, M.A. Drweesh, S.N.S. Youssef, Evaluation of some intercalation methods of dimethylsulphoxide onto HCl-treated and untreated Egyptian kaolinite, Appl. Clay Sci., 137 (2017) 33–42.
[40] S.G. Nasab, A. Semnani, A. Teimouri, M.J. Yazd, T.M. Isfahani, S. Habibollahi, Decolorization of crystal violet from aqueous solutions by a novel adsorbent chitosan/nanodiopside using response surface methodology and artificial neural network-genetic algorithm, Int. J. Biol. Macromol., 124 (2018) 429–443.
[41] R. Zhua, Q. Chen, H. Liu, F. Ge, L. Zhu, J. Zhu, H. He, Montmorillonite as a multifunctional adsorbent can simultaneously remove crystal violet, cetyltrimethylammonium, and 2-naphthol from water, Appl. Clay Sci., 88 (2014) 33–38.
[42] B.D. Mistry, A Handbook of Spectroscopic Data Chemistry (UV, JR, PMR, JJCNMR and Mass Spectroscopy), Oxford Book Company, Jaipur, 2009.
[43] Y. Marcus, The Properties of Solvents, Wiley Series in Solution Chemistry, Wiley, Chichester, 1998.
[44] D.M. Porter, W.S. Brey, Nuclear magnetic resonance studies of hydrogen bonding. II. The pyrrole-dimethyl sulfoxide system, J. Phys. Chem., 72 (1968) 650–654.
[45] X.F. Tan, Y.G. Liu, Y.L. Gu, S.B. Liu, G.M. Zeng, X. Cai, X.J. Hu, H. Wang, S.M. Liu, L.H. Jian, Biochar pyrolyzed from MgAl-layered double hydroxides pre-coated ramie biomass (*Boehmeria nivea* (L.) Gaud.): characterization and application for crystal violet removal, J. Environ. Manage., 184 (2016) 85–93.